Correspondence to:
K. Imai,
imai.koji@jaxa.jp

SMILES observations of mesospheric ozone during the solar eclipse

Koji Imai[1], Takashi Imamura[2], Kenshi Takahashi[3], Hideharu Akiyoshi[2], Yousuke Yamashita[2], Makoto Suzuki[1], Ken Ebisawa[1], and Masato Shiotani[1,3]

[1]Institute of Space and Astronautical Science, Japan Aerospace Exploration Agency, Sagamihara, Japan, [2]National Institute for Environmental Studies, Tsukuba, Japan, [3]Research Institute for Sustainable Humanosphere, Kyoto University, Uji, Japan

Abstract The Superconducting Submillimeter-Wave Limb-Emission Sounder (SMILES) successfully observed vertical distributions of ozone (O_3) concentration in the middle atmosphere during the annular solar eclipse that occurred on 15 January 2010. In the mesosphere, where the photochemical lifetime of O_3 is relatively short (approximately 100 s), altitude-dependent changes in O_3 concentration under reduced solar radiation and their temporal variations were clearly observed as a function of the eclipse obscuration. This study reports the vertical distributions of mesospheric O_3 during a solar eclipse event and analyzes theoretically the eclipse-induced changes. We show that simple analytical expressions for O_3 concentration, which assume that O_3 and O are in a photochemically steady state, can be used to describe the O_3 concentration under reduced solar radiation. The SMILES data obtained during the eclipse provide a unique opportunity to test our current understanding of mesospheric O_3 photochemistry.

1. Introduction

Atmospheric ozone (O_3) plays an important role in determining the thermal and dynamical structure of the middle atmosphere through radiative and chemical processes. To monitor the global distribution of O_3 and related trace gases, the Superconducting Submillimeter-Wave Limb-Emission Sounder (SMILES) was developed and deployed on the Japanese Experiment Module of the International Space Station (ISS) [*Kikuchi et al.*, 2010]. The unprecedented high-sensitivity measurements made using the 4 K cooled submillimeter limb sounder provided new insights into the physics and chemistry of the middle atmosphere such as the diurnal variation in stratospheric O_3 [*Imai et al.*, 2013; *Sakazaki et al.*, 2013; *Parrish et al.*, 2014]. Although the observation period was limited to the period 12 October 2009 to 21 April 2010, SMILES successfully observed a sequence of O_3 profiles during the annular solar eclipse that occurred on 15 January 2010.

Photochemistry in the middle atmosphere related to the production and partitioning of O_X (O and O_3) has been explained in terms of O–O_2–O_3 chemistry, and the loss of O_X is controlled by catalytic chain reactions in addition to the reaction between O and O_3. In the mesosphere, chain reactions involving HO_X (H, OH, and HO_2) radicals are believed to be a dominant driver of O_X loss [e.g., *Allen et al.*, 1984; *Brasseur and Solomon*, 2005]. Although the mesospheric O_X photochemistry seems to be relatively simple, and the chemical lifetime of O_X is much shorter (≤ 1 h) [*Brasseur and Solomon*, 2005] than characteristic transport lifetimes, discrepancies between observed and modeled O_3 concentrations have been reported [e.g., *Sandor et al.*, 1997; *Siskind et al.*, 2013; *Smith et al.*, 2006].

Eclipse-induced changes in spectral solar intensity outside the atmosphere are insensitive to wavelength [*Koepke et al.*, 2001]. Furthermore, the optical depth in the visible and ultraviolet region over the mesosphere is mainly determined by molecular oxygen, and changes in the optical path length of the solar radiation should be small during a solar eclipse. This indicates that when a solar eclipse occurs with a small solar zenith angle (SZA) the temporal change in solar irradiance during the eclipse shows much simpler behavior, from the viewpoint of wavelength distribution, than it does during the sunrise/sunset period, when a relatively large SZA strongly affects the wavelength distribution. Moreover, the ratio of molecular photolysis rates during the eclipse to those before or after the eclipse is almost independent of the effective wavelength for photolysis. It is, therefore, expected that O_3 measurements during the eclipse may provide unique information on O_3 photochemistry in the mesosphere where clear diurnal O_3 variations have been recognized [*Ricaud et al.*, 1996; *Brasseur and Solomon*, 2005; *Imai et al.*, 2013].
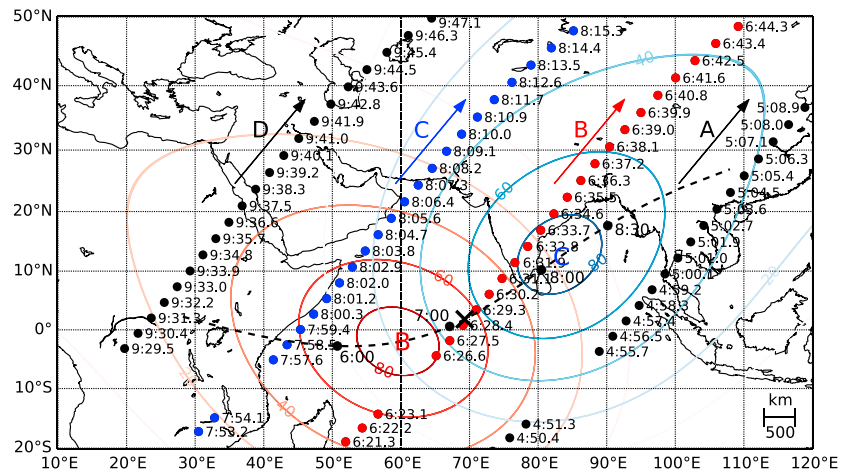
Figure 1. Longitude-latitude section of SMILES observation points with times (UTC) along four paths around the solar eclipse event on 15 January 2010. The center of the Moon's antumbra traveled along the dashed line with times given at black dots. For path B, the observation points are indicated by red dots and the magnitude of the eclipse (%) at 06:29 is also drawn in red contours; the same for path C, but at 08:09 and in blue dots and contours.

To date, there have been no comprehensive detailed observations or analysis of mesospheric O_3 during solar eclipses. Most previous studies have focused on the vertical O_3 distribution in the stratosphere [*Ratnam et al.*, 2011; *Kumar et al.*, 2011; *Manchanda et al.*, 2012] or total column O_3 [*Chakrabarty et al.*, 1997; *Zerefos et al.*, 2000; *Chudzynski et al.*, 2001; *Tzanis*, 2005]. Only a few observations of mesospheric O_3 during solar eclipses have been reported [e.g., *Randhawa*, 1968; *Agashe and Rathi*, 1982; *Connor et al.*, 1994; *Kulikov et al.*, 2008], but they were not robust, and little theoretical analysis of the data was performed. Observations of O_3 changes in the mesosphere as a function of the eclipse obscuration (the fraction of the Sun's area occulted by the Moon) are required if we are to test the current understanding of mesospheric O_3 photochemistry.

The high performance of the SMILES measurements allowed us to successfully obtain changing O_3 profiles during the annular solar eclipse that occurred on 15 January 2010. In this paper, we present clear observational results of O_3 variations in the mesosphere caused by the solar eclipse. We also discuss the altitude-dependent response of O_3 concentration under solar radiation changes in terms of steady state approximations of the photochemistry.

2. SMILES Observations During the Eclipse

SMILES nominally covered the latitudes from 38°S to 65°N on each orbit within a 93 min period. The antenna was scanned in elevation at a period of 53 s with three specified detection bands (Bands A, B, and C) within the submillimeter-wave region [*Kikuchi et al.*, 2010]. During the eclipse event Band B data were available for the O_3 retrieval based on version 2.4 processing (Japanese Experiment Module/Superconducting Submillimeter-Wave Limb-Emission Sounder L2 Products Guide for v2.4, 2013, http://darts.isas.jaxa.jp/iss/smiles/docs/L2dataGuide_2-4.pdf).

Figure 1 shows the SMILES observation points, together with times, along four ascending tracks (Paths A, B, C, and D) around the eclipse event. The antumbra (part of the Moon's shadow) traversed a considerable distance from the westernmost Central African Republic at 05:14 to the Shandong Peninsula, China, at 08:59. All times are expressed in UTC hereafter if not otherwise specified; local times around the four paths are about 10:00–14:00. The track is approximately 12,900 km long and covered a period of 4 h and 15 min, as indicated by the dashed line. Therefore, the solar eclipse could be captured along Paths B and C.

Figure 1 also shows distributions of the eclipse magnitude (the fraction of the Sun's diameter occulted by the Moon, expressed as a percentage) at 06:29 and 08:09 corresponding to Paths B and C, respectively. While the antumbra was crossing the Arabian Ocean as the eclipse magnitude was reaching its maximum, the SMILES observation (Path B) passed close to the maximum. The greatest eclipse magnitude of 91.9% occurred at 07:06.55 over the Arabian Ocean (1.62°N, 69.29°E; denoted by a black cross), and the annular
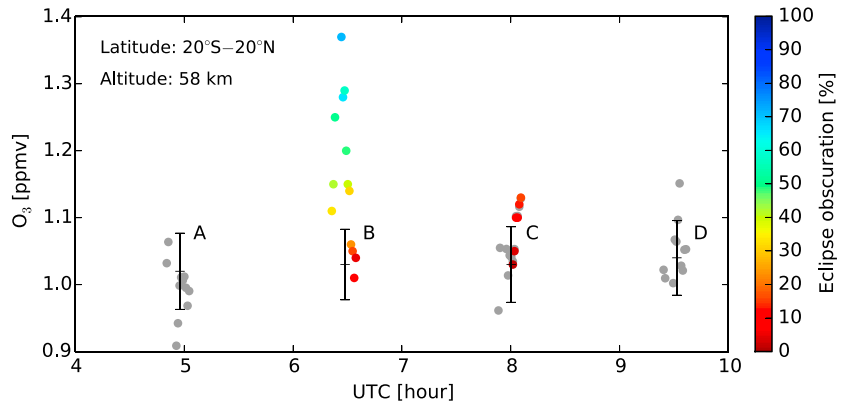
Figure 2. O_3 concentrations measured along the four paths (A, B, C, and D shown in Figure 1) as a function of UTC at 58 km altitude between 20°S and 20°N. The data during the eclipse are colored using eclipse obscuration (%) as shown in the color bar on the right. The grey dots represent the measurements outside the eclipse. Vertical bars indicate the mean and σ of the daytime O_3 concentrations (0° < solar zenith angle (SZA) < 60°) averaged over 60° longitude centered on each path, and between 20°S and 20°N for 4 days, 13–16 January, excluding the data during the eclipse.

eclipse lasted for 11 min and 8 s. On the next path (C), the center of the antumbra was located around 13°N, 83°E, and SMILES also observed the area with an eclipse magnitude of less than 36% at around 30°N. The lack of SMILES measurements at around 10°S was caused by interference from the ISS solar paddle [*Kikuchi et al.*, 2010].

3. Observational Results

Figure 2 shows O_3 concentrations from the SMILES observations for Paths A, B, C, and D at 58 km between 20°S and 20°N. There are clear increases in the O_3 concentrations along Path B near the central antumbra, and slight enhancements along Path C. The daytime mean and 1 standard deviation (σ) values also shown for the corresponding longitude bands of the four paths (see details in the figure caption) indicate that longitudinal variations in the O_3 mixing ratio are small and that the high values along Path B are significant. For values of eclipse obscuration up to about 20%, the O_3 concentrations along Path C are larger than those on Path B, and this might be caused by latitudinal variations.
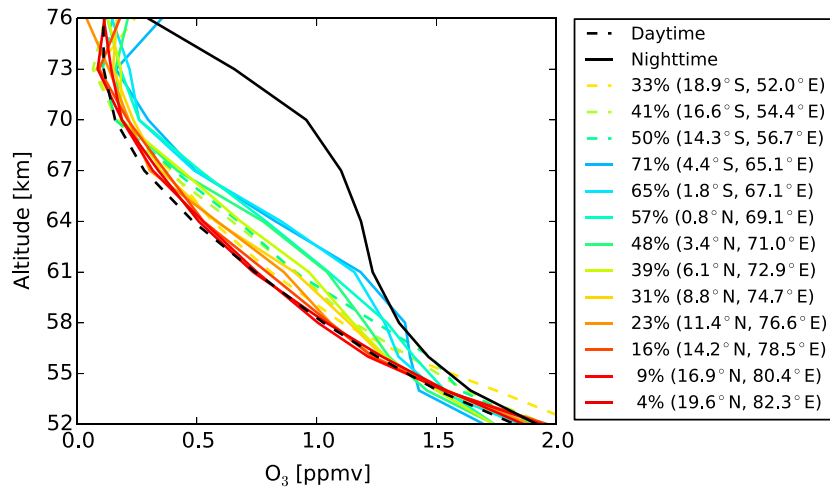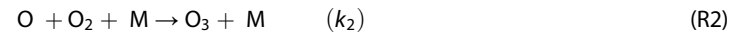

Figure 3. Vertical profiles of O_3 during the eclipse for path B using the same color scale as Figure 2. Profile location and corresponding eclipse obscuration are shown in the legend; the dashed lines are for the southern part of the eclipse center. The black solid and dashed lines are the mean daytime and nighttime profiles of O_3 concentration, respectively. The nighttime mean is defined similarly to the daytime mean in Figure 2 but for the profiles in the range 120° < SZA < 180°.

Figure 3 shows vertical O_3 profiles along Path B between 20°S and 20°N during the eclipse, together with two profiles for the daytime and nighttime means around this latitude band. This indicates that changes in O_3 concentration during the eclipse depend on altitude. For example, at 58 km the maximum O_3 concentration during the eclipse was 40% higher than the daytime average and was almost the same as the nighttime average. In contrast, at 67 km the maximum O_3 concentration during the eclipse was 50% higher than the daytime average, which corresponds to approximately 30% of the typical diurnal variations.

4. Discussion

As described in section 1, O_3 and the O atoms are produced by the following reactions:

$$O_2 + hv \rightarrow 2O \quad (J_1) \tag{R1}$$

$$O + O_2 + M \rightarrow O_3 + M \quad (k_2) \tag{R2}$$

$$O_3 + hv \rightarrow O + O_2 \quad (J_3) \tag{R3}$$

where J_1 and J_3 denote the photolysis rates for reactions (R1) and (R3), respectively, and k_2 the rate coefficient for reaction (R2). During daytime in the mesosphere, O_3 is lost predominantly via reaction (R3), but the following reactions of O_3 with O and H atoms also make minor contributions:

$$O + O_3 \rightarrow 2O_2 \quad (k_4) \tag{R4}$$

$$H + O_3 \rightarrow OH + O_2 \quad (k_5) \tag{R5}$$

The lifetime of O_3 is estimated to be around 100 s [*Brasseur and Solomon*, 2005], short enough to apply the photochemical steady state approximation (SSA) for O_3 concentration:

$$k_2[O][O_2][M] = J_3[O_3] \tag{1}$$

The O atom is lost not only by reaction (R2) but also by reactions with OH and HO_2 radicals:

$$O + OH \rightarrow H + O_2 \quad (k_6) \tag{R6}$$

$$O + HO_2 \rightarrow OH + O_2 \quad (k_7) \tag{R7}$$

Here we assume the SSA holds for the O atom concentration:

$$[O] \approx \frac{J_1[O_2]}{k_X[X]}, \tag{2}$$

where X denotes OH and HO_2 radicals, and k_X the effective rate constant for reactions (R6) and (R7). From equations (1) and (2), the daytime O_3 concentration can be expressed as follows:

$$[O_3] \approx \frac{J_1}{J_3} \cdot \frac{k_2[O_2]^2[M]}{k_X[X]}. \tag{3}$$

As described above, the major species for O_X loss in the mesosphere are HO_2 and OH. The production of HO_X radicals is dominated by photolysis of H_2O in the middle and upper mesosphere [*Brasseur and Solomon*, 2005]:

$$H_2O + hv \rightarrow H + OH \quad (J_8) \tag{R8}$$

In the lower mesosphere and the stratosphere, the reaction of H_2O with $O(^1D)$ becomes dominant:

$$O(^1D) + H_2O \rightarrow 2OH \quad (k_9) \tag{R9}$$
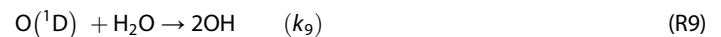
On the other hand, the loss of HO_X is mainly controlled by the following reaction:

$$OH + HO_2 \rightarrow H_2O + O_2 \quad (k_{10}) \tag{R10}$$
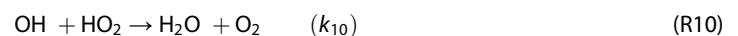
Taking into account the photochemical processes described above, we can rewrite equation (3) as reported by *Allen et al.* [1984]:

$$[O_3] \approx \frac{J_1}{J_3\sqrt{J_8}} \cdot \frac{k_2\sqrt{k_{10}}[O_2]^2[M]}{\sqrt{k_6 k_7 [H_2O]}} \qquad \text{for (R8)-dominant region} \qquad (4)$$

$$[O_3] \approx \sqrt[3]{\frac{J_1{}^2}{J_3{}^3\,\Phi} \cdot \frac{k_2{}^2 k_{10} k_{11}[O_2]^4[M]^3}{k_6 k_7 k_9 [H_2O]}} \qquad \text{for (R9)-dominant region} \qquad (5)$$

where Φ is the quantum yield for $O(^1D)$ production in (R3) and k_{11} is the rate coefficient for physical quenching reaction of $O(^1D)$ atoms produced from (R3).

$$O(^1D) + M \rightarrow O + M \qquad (k_{11}) \qquad (R11)$$

During the eclipse event, the SMILES observations were made near the middle of the day and the observed eclipse only occurred for several hours along the flight path. Thus, the SZA ranged from 25° to 44° during the observations. Accordingly, we assume that the reduction in solar flux during the observed eclipse was determined by the eclipse obscuration, with no significant change in the wavelength distribution. The molecular photolysis rates at fixed SZA during the eclipse are thus calculated by the following:

$$J_i(\eta) = (1-\eta)\cdot J_i(0), \qquad i = 1,\ 3,\ \text{and } 8 \qquad (6)$$

where η is the eclipse obscuration and $J_i(0)$ is the photolysis rate under normal (noneclipse) conditions.

For the eclipse studied here, the maximum obscuration during the SMILES observation was 71%, indicating that the photolysis lifetime for O_3 is estimated to be approximately 6 min. Thus, the SSA was also applied to the O_3 and O concentrations during the observed eclipse. By applying equation (6) to equations (4) and (5), the ratio of the O_3 concentration between the eclipse and normal daytime can be given as a function η:

$$\frac{[O_3](\eta)}{[O_3](0)} \approx (1-\eta)^{-1/2} \qquad (7)$$

$$\frac{[O_3](\eta)}{[O_3](0)} \approx (1-\eta)^{-1/3} \qquad (8)$$

Equation (7) should describe the η dependence of O_3 concentration at altitudes where reaction (R8) dominates as the HO_X source, whereas equation (8) should apply at altitudes where reaction (R9) is dominant. Thus, at 67 km the ratio $[O_3](\eta)/[O_3](0)$ is expected to show an inverse half-power dependence on the solar flux, whereas at lower altitudes, for example, at 58 km, the ratio will shift to an inverse one-third power dependence.

In Figure 4 the SMILES measurements in the lower and upper mesosphere are compared with the inverse one-third power and the inverse half-power dependence. As the sensitivity of the SMILES measurement decreases with increasing height and the resulting profiles sometimes oscillate in the upper mesosphere, the data from 67 and 70 km were averaged. At 67–70 km, the SMILES data closely follow the inverse half-power dependence, whereas at 58 km they are close to the inverse one-third power dependence; least squares fit analysis of the data points gives the slope as 0.51 at 67–70 km and 0.23 at 58 km. We also plotted the SMILES data at 61 and 64 km (not shown) and calculated slopes of 0.50 at 64 km and 0.39 at 61 km. The decreasing trend in the exponents of the power law at altitudes less than about 64 km results from a rapid increase in the HO_X production rate through reaction (R9), and a moderate decrease through reaction (R8) [*Allen et al.*, 1984].

Previous studies of the effects of solar eclipses on atmospheric O_3 have mostly considered the vertical distribution in the stratosphere or the total column O_3. Although a few observations of mesospheric O_3 during solar eclipses have been reported, there has been little theoretical analysis of the observational data. The present study reports a theoretical understanding of the eclipse-induced changes in mesospheric O_3. It was very fortunate that the ISS track encountered the solar eclipse event, and the SMILES observations successfully captured the altitude-dependent changes in mesospheric O_3 concentration from single scan measurements. Note also that because the SZA remained relatively small throughout the event, the conditions under reduced solar radiation were suitable for a simple theoretical
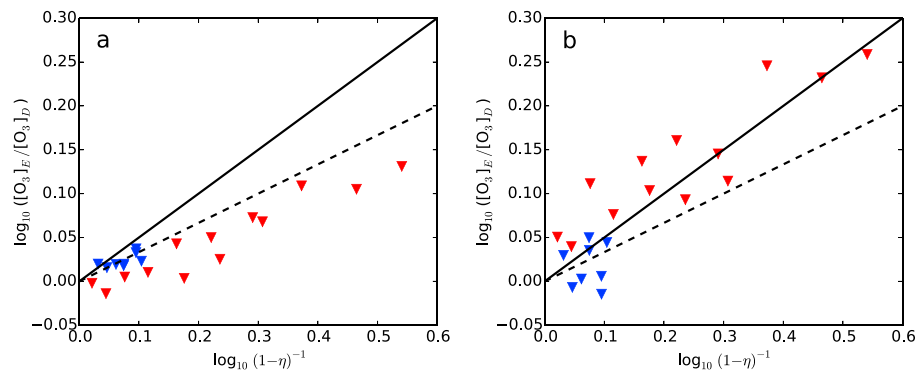
Figure 4. Ratio of the O_3 concentrations during the eclipse and in normal daytime as observed along Paths B (red) and C (blue) at (a) 58 km and (b) 67–70 km (averaged) as a function of the eclipse obscuration. The solid and dashed lines indicate the inverse half-power and the inverse one-third power dependencies, respectively, on the eclipse obscuration, as derived from the analytical expressions (equations (7) and (8)) describing the daytime O_3 concentration under the photochemical steady state approximation (see text).

treatment. The SMILES observations have thus provided a unique data set that enabled us to verify our current understanding of O_3 photochemistry in the daytime mesosphere.

Finally, we note that as described in section 1, there have been some papers reporting discrepancies between observed and modeled O_3 concentrations in the mesosphere [e.g., *Sandor et al.*, 1997; *Siskind et al.*, 2013; *Smith et al.*, 2006]. Although optimization of the kinetic parameters for photochemical reactions involving O_x and HO_x has been suggested to solve the unsettled issue, no firm conclusion has been reached. To study the issue, further analysis could be conducted based on our method presented here, if more profile data for O_3 (and related species) during eclipse events were accumulated. On the other hand, the SMILES observations yielded a large amount of the data for normal diurnal variations in the mesospheric O_3 and related species. Detail analysis of those data is now underway in our group, which is expected to contribute to the issue.

5. Conclusion

In this paper, we have attempted to explain theoretically the SMILES-observed altitude-dependent changes in mesospheric O_3 concentration during the annular solar eclipse that occurred on 15 January 2010. We have shown that simple expressions describing the daytime O_3 concentration under photochemical steady state approximations can be used to analyze the eclipse-induced changes in O_3 concentration, providing a unique opportunity to verify our current knowledge of the key chemical processes involving odd oxygen and HO_X radicals in the daytime mesosphere. Hitherto, testing our understanding of the mesospheric photochemistry mostly involved evaluating the consistency of diurnal variations in O_3 and HO_X concentrations between the observations and model calculations. This study has highlighted that highly sensitive, altitude-resolved measurements of mesospheric O_3 under reduced solar radiation can provide valuable data to test our understanding of the chemical processes in the daytime mesosphere.

References

Agashe, V. V., and S. M. Rathi (1982), Changes in the concentration of mesospheric ozone during the total solar eclipse, *Planet. Space Sci.*, *30*, 507–513, doi:10.1016/0032-0633(82)90061-7.

Allen, M., J. I. Lunine, and Y. K. Yung (1984), The vertical distribution of ozone in the mesosphere and lower thermosphere, *J. Geophys. Res.*, *89*(D3), 4841–4872, doi:10.1029/JD089iD03p04841.

Brasseur, G., and S. Solomon (2005), *Aeronomy of the Middle Atmosphere*, 3rd ed., Springer, Dordrecht, Netherlands.

Chakrabarty, D. K., N. C. Shah, and K. V. Pandya (1997), Fluctuation in ozone column over Ahmedabad during the solar eclipse of 24 October 1995, *Geophys. Res. Lett.*, *24*, 3001–3003, doi:10.1029/97GL03016.

Chudzynski, S., et al. (2001), Observation of ozone concentration during the solar eclipse, *Atmos. Res.*, *57*(1), 43–49, doi:10.1016/S0169-8095(00)00071-5.

Connor, B. J., D. E. Siskind, J. J. Tsou, A. Parrish, and E. E. Remsberg (1994), Ground-based microwave observations of ozone in the upper stratosphere and mesosphere, *J. Geophys. Res.*, *99*(D8), 16,757–16,770, doi:10.1029/94JD01153.

Imai, K., et al. (2013), Validation of ozone data from the Superconducting Submillimeter-Wave Limb-Emission Sounder (SMILES), *J. Geophys. Res. Atmos.*, *118*, 5750–5769, doi:10.1002/jgrd.50434.

Kikuchi, K., et al. (2010), Overview and early results of the Superconducting Submillimeter-Wave Limb-Emission Sounder (SMILES), *J. Geophys. Res.*, *115*, D23306, doi:10.1029/2010JD014379.

Koepke, P., J. Reuder, and J. Schween (2001), Spectral variation of the solar radiation during an eclipse, *Meteorol. Z.*, *10*(3), 179–186, doi:10.1127/0941-2948/2001/0010-0179.

Kulikov, Y. Y., A. A. Krasil'nikov, V. M. Demkin, and V. G. Ryskin (2008), Variations in the concentration of mesospheric ozone during the total solar eclipse of March 29, 2006, from microwave radiometric data, *Izv. Atmos. Oceanic Phys.*, *44*, 486–490, doi:10.1134/S0001433808040099.

Kumar, K. K., K. V. Subrahmanyam, and S. R. John (2011), New insights into the stratospheric and mesosphere-lower thermospheric ozone response to the abrupt changes in solar forcing, *Ann. Geophys.*, *29*, 1093–1099, doi:10.5194/angeo-29-1093-2011.

Manchanda, R. K., P. R. Sinha, S. Sreenivasan, D. B. Trivedi, B. V. N. Kapardhi, B. S. Kumar, P. R. Kumar, U. Satyaprakash, and V. N. Rao (2012), In-situ measurements of vertical structure of ozone during the solar eclipse of 15 January 2010, *J. Atmos. Sol. Terr. Phys.*, *84–85*, 88–100, doi:10.1016/j.jastp.2012.05.011.

Parrish, A., et al. (2014), Diurnal variations of stratospheric ozone measured by ground-based microwave remote sensing at the Mauna Loa NDACC site: Measurement validation and GEOSCCM model comparison, *Atmos. Chem. Phys.*, *14*, 7255–7272, doi:10.5194/acp-14-7255-2014.

Randhawa, J. S. (1968), Mesospheric ozone measurements during a solar eclipse, *J. Geophys. Res.*, *73*(2), 493–495, doi:10.1029/JB073i002p00493.

Ratnam, M. V., G. Basha, M. Roja Raman, S. K. Mehta, B. V. Krishna Murthy, and A. Jayaraman (2011), Unusual enhancement in temperature and ozone vertical distribution in the lower stratosphere observed over Gadanki, India, following the 15 January 2010 annular eclipse, *Geophys. Res. Lett.*, *38*, L02803, doi:10.1029/2010GL045903.

Ricaud, P., J. deLa Noë, B. J. Connor, L. Froidevaux, J. W. Waters, R. S. Harwood, I. A. MacKenzie, and G. E. Peckham (1996), Diurnal variability of mesospheric ozone as measured by the UARS microwave limb sounder instrument: Theoretical and ground-based validations, *J. Geophys. Res.*, *101*(D6), 10,077–10,089, doi:10.1029/95JD02841.

Sakazaki, T., et al. (2013), Diurnal ozone variations in the stratosphere revealed in observations from the Superconducting Submillimeter-Wave Limb-Emission Sounder (SMILES) on board the International Space Station (ISS), *J. Geophys. Res. Atmos.*, *118*, 2991–3006, doi:10.1002/jgrd.50220.

Sandor, B. J., R. T. Clancy, D. W. Rusch, C. E. Randall, R. S. Eckman, D. S. Siskind, and D. O. Muhleman (1997), Microwave observations and modeling of $O_2(^1\Delta_g)$ and O_3 diurnal variation in the mesosphere, *J. Geophys. Res.*, *102*(D7), 9013–9028.

Siskind, D. E., M. H. Stevens, C. R. Englert, and M. G. Mlynczak (2013), Comparison of a photochemical model with observations of mesospheric hydroxyl and ozone, *J. Geophys. Res. Atmos.*, *118*, 195–207, doi:10.1029/2012JD017971.

Smith, G. P., M. Frenklach, R. Feeley, A. Packard, and P. Seiler (2006), A system analysis approach for atmospheric observations and models: Mesospheric HOx dilemma, *J. Geophys. Res.*, *111*, D23301, doi:10.1029/2005JD006846.

Tzanis, C. (2005), Ground-based observations of ozone at Athens, Greece during the solar eclipse of 1999, *Int. J. Remote Sens.*, *26*, 3585–3596, doi:10.1080/01431160500076947.

Zerefos, C. S., et al. (2000), Changes in surface solar UV irradiances and total ozone during the solar eclipse of August 11, 1999, *J. Geophys. Res.*, *105*(D21), 26,463–26,473, doi:10.1029/2000JD900412.